Journal of Alloys and Compounds 598 (2014) 177–183

Contents lists available at ScienceDirect

Journal of Alloys and Compounds

journal homepage: www.elsevier.com/locate/jalcom

Effect of substrate temperature on the characteristics of α-MoO_3 hierarchical 3D microspheres prepared by facile PVD process

Rabindar K. Sharma *, G.B. Reddy

Thin Film Laboratory, Department of Physics, Indian Institute of Technology Delhi, New Delhi 110016, India

ARTICLE INFO

Article history:
Received 16 August 2013
Received in revised form 17 January 2014
Accepted 31 January 2014
Available online 8 February 2014

Keywords:
Microspheres
Nanoflakes
Plasma assisted growth
Thermal evaporation

ABSTRACT

The authors report the fabrication of morphologically controlled α-MoO_3 hierarchical microspheres (MS_s) with the nanoflakes (NF_s) on nickel coated glass substrate using a facile low cost physical vapor deposition (PVD) routes without any template or surfactant. The synthesis mechanism of MS_s includes the sequences of plasma assisted sublimation and thermal evaporation processes in three independent steps. It is experimentally demonstrated that the nanostructured thin film with vertically aligned NF_s during first growth step provides a seed layer for the growth of MS_s. The morphological, structural, and optical properties of MoO_3 MS_s are investigated systematically as function of substrate/growth temperatures. The obtained results endorse the surface morphology of α-MoO_3 MS_s are strongly depending on the growth temperature at the final growth step. HRTEM analysis with SAED assured that NF_s existing on the surface of MoO_3 MS_s are single crystalline in nature. The vibrational study of molybdenum and oxygen atoms in MS_s is carried out by micro-Raman and infra-red (IR) spectroscopy, which evident the presence of single orthorhombic phase of MoO_3 MS_s and agreed with XRD results. The MoO_3 MS_s exhibit photoluminescence (PL) in the UV–visible region at room temperature and the emission is observed to be strongly enhanced with the increase of substrate/growth temperature in accordance with the improvement in the degree of crystallinity characterized by XRD analysis.

1. Introduction

It is conceived that there is a very close relationship between the morphology and the properties of inorganic materials. For example, isotropic and anisotropic behavior is strongly related to the size, shape and dimensionality of the materials [1]. As a result there has been considerable effort in synthesizing inorganic materials with controlled shapes of architectures, which are desirable for many applications in optics, electronics and in energy storage devices. In particular, the alignment of nanostructure building blocks or the structure morphology on the surface of inner core (nanoparticles, nanorods, and nanoflakes) into three dimensional (3D) ordered microstructures by bottom-up approaches has been an exciting field in recent years for new technological applications [2]. To date, a wide variety of inorganic materials, including metal, metal oxide, sulfide and other materials have been successfully synthesized with hierarchical shapes [3–8]. Among all transition metal oxides with diverse morphological structure have a wide range of potential applications. Specifically, nanostructured transition metal oxides are of significant interest due to their applications in the field of sensors, photo-catalysis, electrochromic, field emission and solar energy devices [9–11]. As a wide band gap semiconducting material molybdenum oxide (MoO_3) has received considerable attention over the past few years owing to its diverse application in various fields such as elements for the information display, energy-efficient window technology, optical switching coating, high density memory devices, gas sensors, heterogeneous catalysis and positive negative photo resistivity [12–17]. The variety of MoO_3 nanostructures, such as nanowires, nanotubes, nanobelts, nanostars, nanorods, nanoflakes, and nanospheres has been prepared by using different routes. Zhou et al. [18] grown α-MoO_3 nanowires by using a thermal evaporation method under vacuum conditions at very high boat temperature 1100 °C on silicon substrates. Diaz-Droquett et al. [19] synthesized the molybdenum trioxide nanostructures such as nanoribbons, nanofibers, nanoniddles and nanoparticles by direct thermal evaporation of MoO_3 powder at high temperatures. Liu et al. have reported the growth of hollow nanospheres of MoO_3 and WO_3 assembled with the polymeric micelles by using a soft template of polymeric micelle with the core–shell–corona architecture [8]. Dense MoO_3 nanoparticles as well as the hollow microspheres are reported so far [20,21], no MoO_3 microspheres with solid inner core by the facile deposition route have been reported. Among the various

* Corresponding author. Tel.: +91 9015977189.
E-mail address: rkrksharma6@gmail.com (R.K. Sharma).

http://dx.doi.org/10.1016/j.jallcom.2014.01.238
0925-8388/

morphological structures mentioned above, hierarchical microspheres, especially those with uniform shape and size have attracted much attention because of their large surface area, mechanical and thermal stabilities. The importance of hierarchical microstructures of metal oxides from the applications point of view, motivates us for the current work. Most of the groups have synthesized hierarchically structured nano/microspheres with the assistance of the templates and surfactants by chemical routes. Although chemical routes work but has some boundaries. For instance, chemical routes are complex, more or less produce contamination, need several steps of washing, purification, and drying, etc. The PVD process demonstrated in this paper is very simple and rapid growth process, which is also benign to the environment, may lead to large-scale industrial production.

In this communication, we present a low cost and controllable physical vapor deposition (PVD) strategy to fabricate hierarchical MoO_3 MS_s on nickel coated glass substrate. The PVD growth strategy basically includes the two different synthesis processes as plasma assisted sublimation process and thermal evaporation route in three individual steps. The morphological and structural studies divulge that the features and the alignment of NF_s on the surface of MS_s are strongly dependent on substrate temperature. At low substrate temperature flakes are randomly aligned on the surface of MS_s, while the flakes assembled and form bunches at relatively high growth temperature due to the surface interactions among these NF_s [22]. The recorded HRTEM and SAED images reveals that the grown flakes are single crystalline in nature and verify the XRD findings. The vibrational study of hierarchical MoO_3 microspheres at the different substrate temperatures is discussed in this paper. The enhanced intensity of PL emission of MS_s with the increase in substrate temperature may be owing to the improvement in the degree of crystallinity. The MoO_3 MS_s are expected to exhibit enhanced functionality, particularly in the form of hierarchical architecture at micro scale because of large surface area, Li^+ ion batteries and gas sensing applications.

2. Experimental details

Molybdenum oxide microspheres (MS_s) have been grown on the nickel coated glass substrates by employing both the plasma assisted sublimation and the thermal evaporation process in three independent growth steps. In first growth step MoO_3 film is deposited on Ni coated glass substrate by plasma assisted sublimation process at 500 °C in oxygen plasma ambience, while second step includes the deposition of MoO_3 film on the pre-deposited substrate by thermal evaporation at room temperature and the third step incorporate the deposition of MoO_3 film on the thermally evaporated MoO_3 film (grown in second step) by the same process as used in first step under the same processing parameters. The schematic diagram of experimental setup of both the deposition mechanisms including the cross-sectional view of deposited films with thickness details is shown in Fig. 1(a–c). First the nickel thin film of thickness about 100 nm was deposited on glass substrate by thermally evaporating (99.99% Aldrich) pure nickel powder at base vacuum of 7.5×10^{-6} Torr. After the deposition of nickel film on glass substrates, in first step the Ni coated glass substrates are mounted in the centre of Mo strip (taking as a sublimation source) and keeping the substrate temperature at 500 °C by suitably adjusting the current, passed through the source. The ratio of substrate area to that of the Mo-strip (8×3) cm^2 was nearly 1/10. The heated Mo strip along with substrate was placed inside the oxygen plasma in first growth step. The plasma parameters on sublimation viz. plasma voltage, electrode separation and oxygen pressure were kept constant at 2500 V, 7.5 cm and 7.5×10^{-2} Torr respectively. After deposition of MoO_3 film (of thickness nearly 1 μm) by plasma assisted sublimation route the sample is allowed to cool naturally at room temperature. In second step molybdenum oxide film of thickness 1.0 μm is deposited on the pre-deposited substrate by thermal evaporation of MoO_3 powder (Merck 99.99%) at a base vacuum of 7.5×10^{-6} Torr at room temperature without oxygen plasma ambience. Last deposition step includes further sublimation of MoO_3 under the same plasma parameters as in first step beside the substrate temperature. The film growth was carried out at three substrate temperatures at 300, 400, and 500 °C in the third step. In all growth steps the deposition duration remain fixed as ½ h. The microstructure of MoO_3 MS_s prepared at different substrate temperature was studied with scanning electron microscope ZEISS EVO Series scanning electron microscope model EVO-50. Structural analysis of the MoO_3 MS_s was carried out using Philips X-ray diffractometer using Cu Kα radiation ($\lambda \sim 1.54$ Å) with glancing angle kept constant at 1°. Vibrational study of molybdenum and oxygen atoms in MS_s was carried out by micro-Raman spectroscopy of Renishaw-inVia (excited with an Ar^+ line at 514.5 nm) and Perkin Elmer (Spectrum BX) FTIR in the spectral range from 200 to 1000 cm^{-1} and 400 to 1200 cm^{-1} respectively. Transmission electron microscopy (TEM) studies of samples were carried out on Philips Model CM12 operated at 120 kV with selected area electron diffraction (SAED) analysis. More insight characterization of MS_s was performed by high-resolution transmission electron microscopy. The photoluminescence (PL) was studies by using a xenon lamp (excited at 250 nm line). The thickness of films after growth in each step is determined by AMBIOS Technology (XP-2) stylus profilometer.

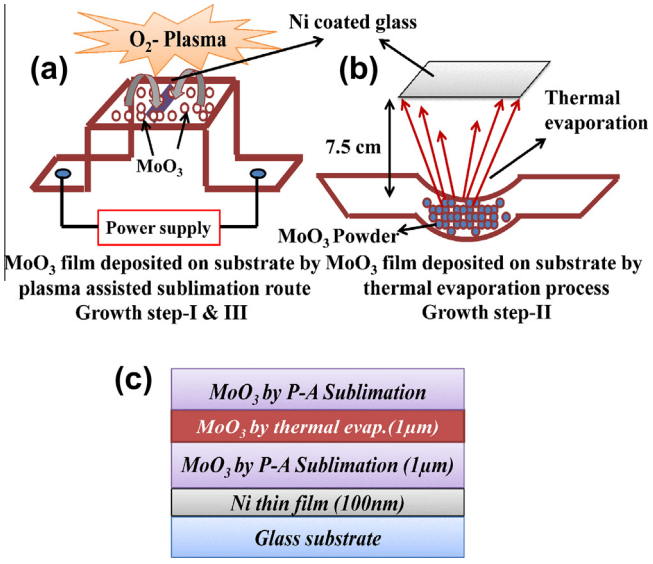

Fig. 1. Schematic diagram of experimental setups employed to grow MoO_3 MS_s: (a) set up used in the plasma assisted sublimation process. (b) Set up used in thermal evaporation process. (c) Cross-sectional view of deposited films during each growth step with the respective thicknesses.

3. Results and discussions

3.1. XRD analysis

X-ray diffraction pattern of MoO_3 nanostructured thin films fabricated at different substrate temperature is shown in Fig. 2. All the recorded diffraction peaks can be clearly assigned as an orthorhombic phase of MoO_3 and matched very well with the reported data (JCPDS card no. 00-005-508, $a = 3.962$ Å, $b = 13.858$ Å and $c = 3.697$ Å). No impurity peaks are observed within the detection limit of X-ray diffraction, indicating that the grown structures as a function of substrate temperature are pure. In XRD pattern, it is worth noting that of film deposited at substrate temperatures

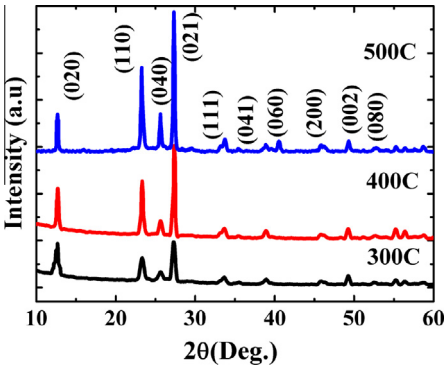

Fig. 2. X-ray diffractograms of MoO_3 films deposited at 300, 400 and 500 °C during final growth step.

300 and 400 °C, the peaks intensity observed from most of the crystal planes of grown nanostructures are considerable, which directly evident the random alignment of grown nanostructures. As the substrate temperature increase to 500 °C, peak corresponding to the crystal planes (1 1 0) and (0 2 1) are dominant and their intensity become relatively higher than the other peaks revealing the highly oriented growth of the formed MoO_3 product rather than random distribution. Additionally, higher intensity and broad spectral width of peaks particularly at low temperature affirms that the crystallite size is very small. The average size of crystalline grains of films deposited at different temperatures is theoretically calculated by using the following Debye–Scherrer formula [23].

$$D_{hkl} = \frac{k\lambda}{\beta(hkl) \cdot \cos(\theta_{hkl})} \quad (1)$$

where D_{hkl} is the average linear dimension of the crystal perpendicular to the diffracting plane ($h\,k\,l$), λ is the wavelength of the incident X-ray beam, θ_{hkl} is the Bragg angle, k is the shape factor with value in neighborhood of 1 and $\beta(hkl)$ is the full width at half maximum (FWHM) in radians of most intense diffraction peaks corrected for the instrumental line broadening. The crystallite sizes are found to 16.8, 26.4, and 39.5 nm for the films deposited at 300, 400, and 500 °C respectively, which confirms the presence of nanocrystallites in the MoO_3 films prepared in this work. The increase in crystallite size with growth temperature reveals the improved crystallinity and decreases the grain boundary discontinuities.

3.2. SEM analysis

The SEM micrograph of deposited MoO_3 film is recorded after every step as well as different substrate temperatures during final step to understand the morphological change. During first step the deposited film shows the formation of vertically aligned nanoflakes see in Fig. 3(a), which provides the favorable environment for the growth of MoO_3 MS_s in our case. After second consecutive growth step islands like morphology originated with smooth surface by thermal evaporation process at room temperature (see in Fig. 3b). The recorded micrographs of finally deposited films confirm the formation of microspheres like morphology and also endorse that the surface structure greatly modified as a function of substrate temperatures during the last growth stage. At high growth temperature islands start to collapse into each other due to the large diffusion rate and transformed in well shaped spheres of relatively large diameter to attain the minimum energy

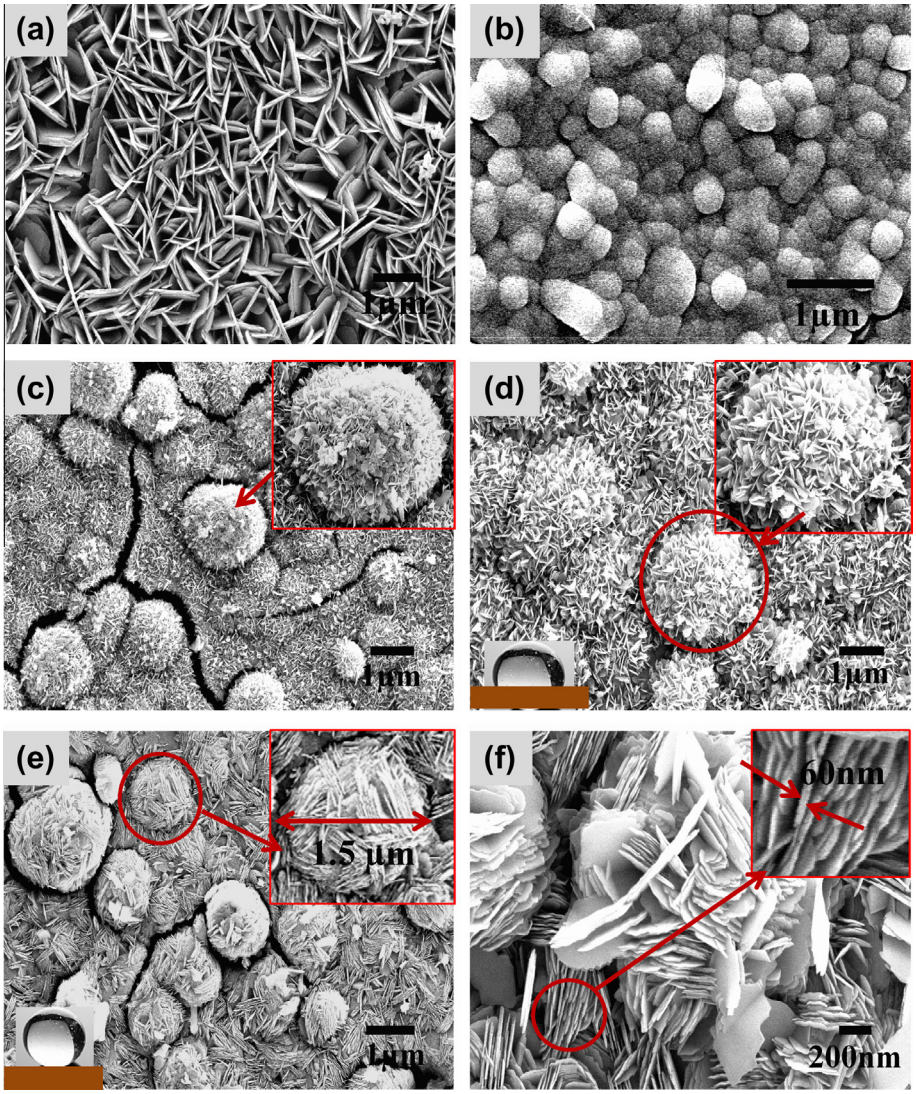

Fig. 3. SEM micrographs: (a) shows the formation of vertically aligned MoO_3 NF_s during first growth step. (b) Shows the islands like morphology of film deposited by thermal evaporation at room temperature. (c) Formation of MS_s at temperature 300 °C. (d) MS_s formed at 400 °C. (e) Low magnification image of film deposited at 500 °C. (f) Magnified view of the same film prepared at 500 °C.

configuration. The finally grown MoO_3 microspheres at all temperatures have rough surface because the coexistence of the well aligned nanoflakes on their surface and the roughness is continuously enhanced due to the increment in flake dimensions with growth temperature. Randomly oriented tiny flakes with the average thickness of 40 nm deposited at 300 °C on MS_s can be seen from Fig. 3(c). These flakes are not developed sufficiently in terms of shape and size at that temperature because of low mobility of incoming MoO_3 molecules, consequently less probability to migrate on substrate and achieve proper nucleation sites for growth, (see inset of Fig. 3(a)). The MS_s prepared at growth temperature 400 °C exhibit densely packed grains and flakes large in size due to the relatively high mobility of incoming MoO_3 molecules at higher temperature, facilitates to crop out the well established flakes on their surfaces can be seen Fig. 3(d) with inset. The low magnification SEM micrograph of sample formed at 500 °C is shown in Fig. 3(e), consists the hierarchically structured MoO_3 MS_s with the completely developed nanoflakes. The surface morphology is quite uniform, confirming the growth process is progressed uniformly on the entire substrate of area (15×20) mm^2. The microsphere with the typical diameter of 1.5 μm is shown in the inset of Fig. 3(c). The obtained MoO_3 microspheres have the diameters in between the range of 0.7–2 μm at all temperatures. The magnified view of the same film deposited at 500 °C is depicted in Fig. 3(f), revealed that every microsphere consists the vertically aligned NF_s with the average thickness of about 60 nm on its surface. The micrographs divulge that the average thickness of flakes is increased with growth temperature. At higher temperature 500 °C flakes lies on the surface of sphere are assembled and form bunches of parallely aligned flakes. It is believed that these bunches of nanoflakes are organized, when more than one flakes come in parallel in close proximity with the gradual enlargement of surface areas due to the surface interactions, can be clearly viewed in the inset of Fig. 3(f). All bunches are not arrayed in same direction on spherical surface but aligned randomly in all the possible directions, which is in completely agreement with the XRD results. The MoO_3 microspheres grown at 500 °C are attained well spherical shape than previous growth temperatures because of the enhanced rate of coalescence of islands formed during second growth step. High substrate temperature during final growth supplies additional thermal energy, which offers high mobility of MoO_3 molecules to migrate on the substrate for accomplishing the preferential heterogeneous nucleation sites and the high coalescence rate of islands, which is the core of grown MS_s in our case. Consequently the well organized microspheres coexisting with nanoflakes are crop out. It is noticed that two growth processes, one is the coalescence of islands and other is the deposition of MoO_3 by sublimation taking place simultaneously during last step at all temperatures. The measured film thicknesses after the previous and second growth steps are found to be nearly same of the order of 1 μm. Finally it is worth to remark that the elevated growth temperature not only assists to grow well shaped nanoflakes on MS_s but also in the coalescence of islands (which is the core of MS_s) those prepared during second growth step to acquire more spherical morphology by the surface energy minimization. The structural and morphological studies confirmed that the hierarchically structured α-MoO_3 microspheres with nanoflakes distributed uniformly on entire substrate offer very large surface area, may be better candidate for applications such as secondary Li^+ ion batteries and gas sensor devices.

3.3. TEM, HRTEM analysis with SAED pattern

We could not analyze the grown microspheres by the transmission electron microscope (TEM) owing to relatively large diameters. The bunches of nanoflakes detached from microspheres surface when they disperse to ethanol with prolonged ultrasonication ~5 h, allowing us to examine these flakes individually at different temperatures. The typical low magnified bright field TEM micrograph of all films deposited at distinct temperatures is shown in Fig. 4, the dark portion in all TEM image is found either of the relatively large size of MS_s or the bunching of nanoflakes with dense and smooth surfaces, which is also consistent with SEM

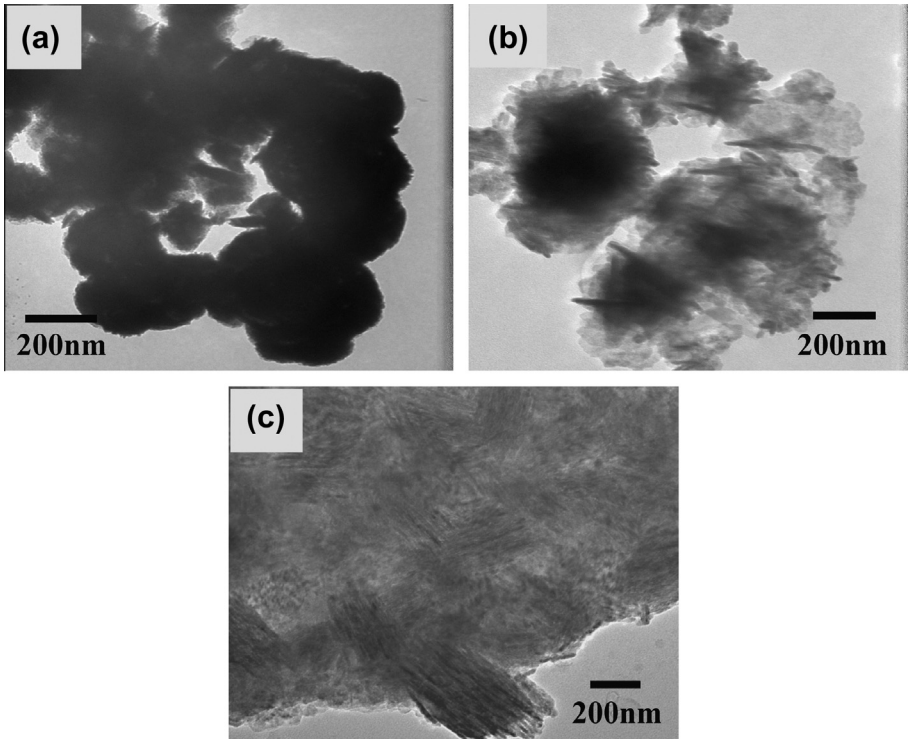

Fig. 4. (a) Low magnification TEM micrographs of MS_s grown at 300, 400 and 500 °C.

result. The MoO_3 NF_s lies on MS_s in case of low substrate temperature (300 °C) are not clearly visualized due to their smaller dimensions relative to the diameter of MS_s (see in Fig. 4a). Whereas the NF_s grown on MS_s at higher temperatures (400 °C and 500 °C) are significantly large in dimensions and the mean thickness of NF_s in both cases are nearly same ~40 nm can be seen in Fig. 4(b and c), which are approximately matched with the crystallite size obtained by the XRD analysis. A typical TEM images at higher magnification of the well separated flakes formed at 400 and 500 °C with the highlighted region for HRTEM measurement are shown in Fig. 5(a and b). Further characterization of MoO_3 nanoflakes of both samples is performed by high resolution electron microscopy (HRTEM) with selected area electron diffraction pattern, divulged that nanoflakes placed on microspheres surface are composed of single crystalline orthorhombic α-MoO_3 with top/bottom surface of [0 1 0] and the growth lying preferentially along [0 2 1] direction. The SAED patterns are obtained by focusing the electron beam perpendicular to the anisotropic growth axis of single MoO_3 NF_s is attributed to the [0 1 0] zone axis diffraction revealed in Fig. 5(c and d), clearly exhibit diffraction spots with the d-spacing that could be indexed according to the orthorhombic crystal structure of α-MoO_3 and indicates that the well crystallized single crystal NF_s are grown along [0 2 1] crystallographic orientation on microspheres in both cases. The magnified images show the clear lattice fringes of individual nanoflakes. These images reveal that the inter planer separation of lattice fringes are 0.335 nm and 0.340 nm, which is consistent with the d spacing of (0 2 1) planes for the orthorhombic phase of MoO_3.

3.4. Raman analysis

Raman spectroscopy is employed to further confirm that the MS_s prepared at different temperatures having only single orthorhombic phase. Raman spectra of MoO_3 MS_s grown at different temperatures show sharp Raman peaks with enhancing intensity as a function of substrate temperature can be seen systematically in Fig. 6. The increase in peak intensities on increasing substrate temperature is evident the improvement in degree of crystallinity and support the SEM and XRD results. The obtained Raman peaks positioned at 235, 285, 330, 370, 658, 810, and, 986 cm^{-1} are corresponds to orthorhombic MoO_3 phase [24]. The vibrational analysis of Raman spectra of MS_s reveals that the bands in the 900–600 and 400–200 cm^{-1} region are mainly owing to the Mo—O stretching and bending modes, respectively. The Raman peaks at 986, 810, and 658 cm^{-1} in MoO_3 microspheres is the characteristics of α-MoO_3. In general, the crystalline structure of orthorhombic α-MoO_3 can be figured as consisting of corner-sharing chains of MoO_6 octahedra, in which one oxygen is unshared, two oxygen atoms are common to two octahedra and three oxygens are in part-shared edges and common to three octahedra [25]. The bond lengths of terminal bond (Mo=O) along *a*- and *b*-directions (1.67 and 1.73 Å) are shorter than Mo—O bond length along the *c*-axis (1.95 Å) [26]. The sharp intense peak at 986 cm^{-1} is assigned to the terminal oxygen (Mo^{6+}=O) stretching mode along *a*- and *b*-axes which is the cause of the layered structure of α-MoO_3 [27]. The bridging oxygens existing along *c*-axis are weakly bound. The generation of oxygen vacancies should therefore lead to anion vacancies along the *c*-axis. Therefore, a Shifting of the Mo atom towards the terminal oxygen in the *b*-direction can be anticipated with the loss of bridging oxygen, thus weakening the terminal bond along the *a*-axis [28]. The Raman peak at 810 cm^{-1} is assigned to the doubly coordinated oxygen (Mo—O—Mo) in stretching mode, which results from corner-shared oxygen in common with two octahedra. The peak located at 658 cm^{-1} is assigned to the triply coordinated oxygen (Mo_3—O) stretching mode which results from edge-shared oxygen in common with three octahedra [29]. The low intense Raman peaks positioned on lower wavenumber side at 235, 285, 330, and 370 cm^{-1} can be attributed to O—Mo—O scissoring and O=Mo=O wagging modes, respectively [30].

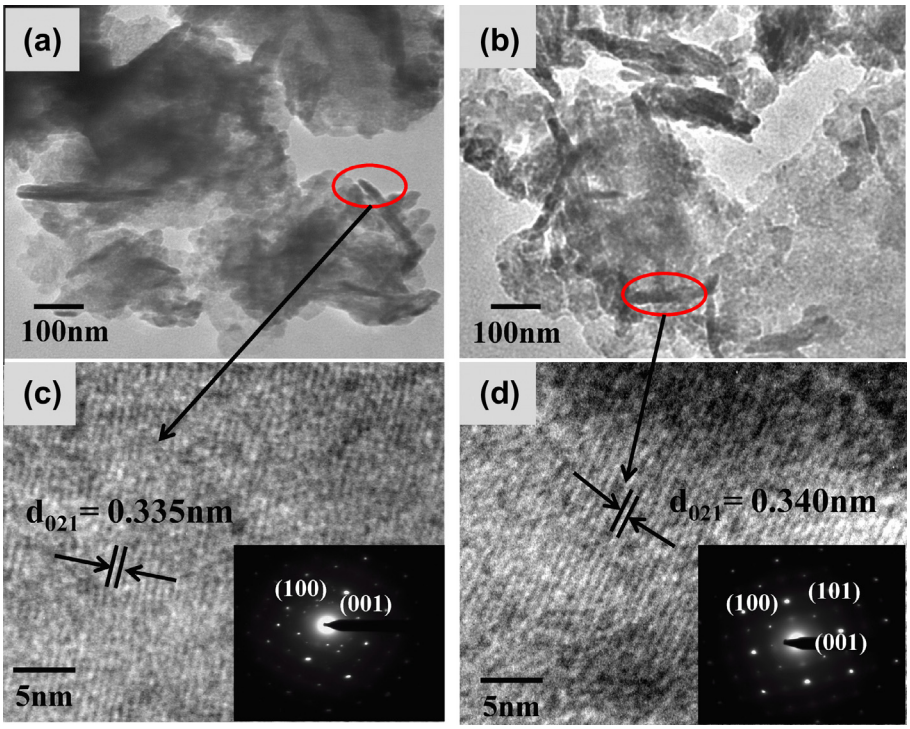

Fig. 5. (a and b) Highly magnified TEM images of individual NF_s formed at 400 and 500 °C (c and d) typical HRTEM images of separated NF_s grown at 400 and 500 °C with their SAED patterns.

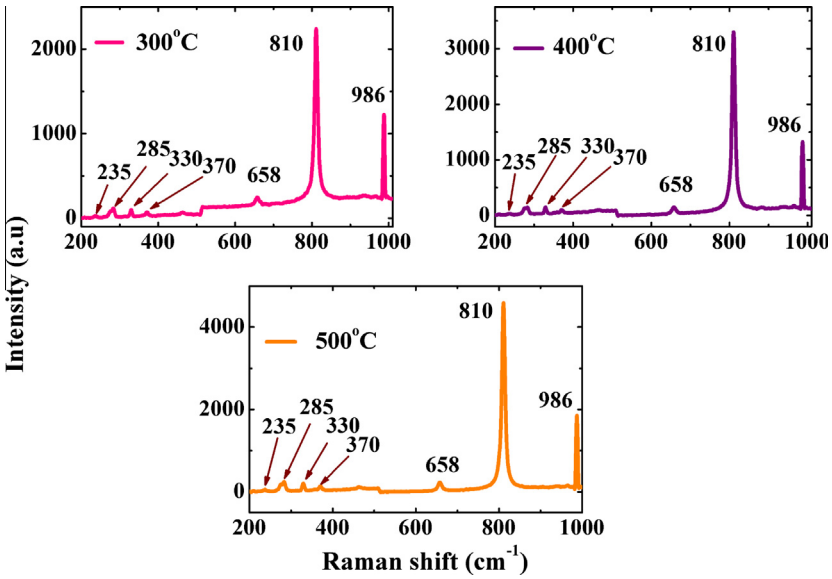

Fig. 6. Raman spectra of MS_s fabricated at growth temperature 300, 400, and 500 °C.

3.5. FTIR analysis

Fig. 7 shows the FTIR spectra of all samples are recorded in the wavenumber range of 400–1100 cm^{-1} further to study the vibrational properties of MoO_3 MS_s. It is revealed from IR spectra that majority of the molecular vibrational frequencies are present in this region of interest. The MoO_3 microspheres formed at different substrate temperature show seven significant absorption peaks positioned at 993, 960, 883, 828, 798, 620, and 502 cm^{-1}.These observed absorption peaks are attributed to different modes of vibrations. The investigation is based on the fact that the MoO_3 is organized by MoO_6 octahedra for which stretching and bending vibrational infrared active modes invariably occur in the 500–1100 cm^{-1} region [31]. As the substrate temperature increases from 300 to 500 °C during last growth step, the IR absorption peaks intensity correspondingly increases, which directly evident the enhancement of nanoflakes dimensions owing to the increase in degree of crystallinity. Two strong absorption peaks located at 883 and 993 cm^{-1}, associated with the stretching mode of oxygen in the Mo—O—Mo mode, and the Mo=O stretching mode, which is the specification of terminal double bonds and confirms the basic characteristic of a layered structure of α-MoO_3 [32]. The absorption peak located at 960 cm^{-1} in all samples attributed the existence of molybdenum species of lower oxidation state i.e. Mo (V) at higher temperature [33] and the weak absorption peak at 828 cm^{-1} is due to the doubly connected bridge oxygen Mo—O—Mo stretching modes corresponding to the asymmetric Mo—O bond length relative to O [32]. The small red shift of the absorption band located in the range of 600–630 cm^{-1} with increasing growth temperature may be either to the presence of molybdenum species of lower oxidation states or due to the thermal disorder in samples, and is assigned the vibration of Mo_2O_2 entity formed by edge shared MoO_6 polyhedra building the orthorhombic α-MoO_3 structure [33]. It can also be noticed that as the substrate temperature increases during final growth step the oxidation as well as the volatilization of MoO_3 start to increase as a result the thickness of MoO_3 films get enhanced in proportionality [34,35]. The intensity of all the IR-absorption peaks gets enhanced with growth temperature owing to the increment in the number density of bonds. The peak located at 798 cm^{-1} in our case is due to the stretching mode of Mo—O—Mo corresponding to the symmetric Mo—O bond length of both the side of O and the peak observed at 502 cm^{-1} is due to the bending mode of Mo—O—Mo entity [32]. The observations obtained from FTIR spectra are in consonance with the Raman and XRD results.

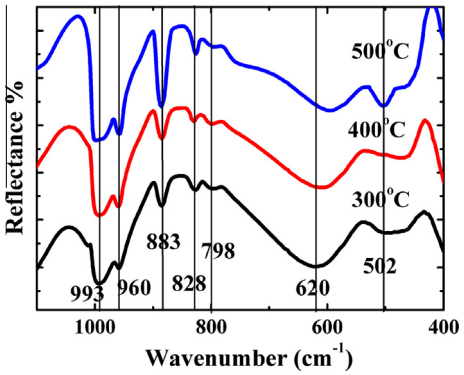

Fig. 7. FTIR spectra of MS_s formed at temperature 300, 400, and 500 °C.

3.6. PL studies

Room temperature PL emission of the MoO_3 MS_s processed at 300, 400, 500 °C substrate temperature is studied in the wavelength range from 300 to 750 nm (with the excitation wavelength/energy is 250 nm/4.97 eV more than the band gap energy) can be seen in Fig. 8. The inset image shows the deconvoluted PL spectra of MS_s grown at 500 °C to clearly specify the emission bands. The PL spectra presented broad peaks over the 380–600 nm range with a strong indigo emission centered at 360–460 nm (P1) in accordance with the report of Song et al. [36], which is corresponding to the near band edge emission (see in the deconvoluted inset of Fig. 8). The other luminescence bands of MoO_3 MS_s obtained at 457, 488, 521, and 535 nm labelled as P2, P3, P4, and P5 respectively may be assigned to the lattice imperfections such as simple oxygen vacancy or some other complex defect such as lower oxidation state (Mo^{5+}) associated with the transfer of charge from oxygen vacancies to Mo ion [37,38]. The PL bands lies at 457 and 488 nm can be attributed to the emission in $Mo^{5+}d^2_{yz}$—d^2_{xz} transition while the less intense PL bands observed at 521 and 535 nm are corresponding to the deep level

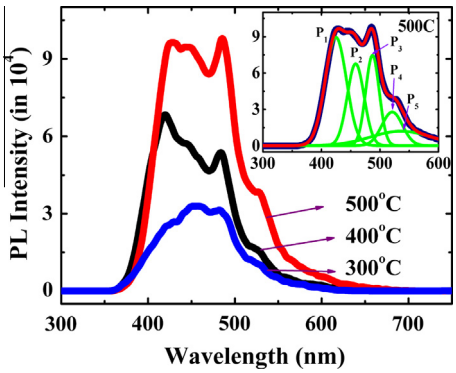

Fig. 8. PL spectra of MoO_3 MS_s at different growth temperatures (inset: Gaussian de-convoluted PL spectrum of sample formed at 500 °C).

$Mo^{5+}d_z^2{}^2$—d_{xy}^2 transitions [39,40]. The existence of these defects in all films is also demonstrated by the FTIR and Raman analysis. The gradual increase in the PL intensity can be seen on increasing the processing temperature from 300 to 500 °C. It is noticed that the obtained PL intensity of MS_s at 500 °C is ~3 times higher than 300 °C. This enhancement in PL emission intensity with substrate temperature can be associated to decrease in the non radiative defects and the increase in the MoO_3 crystallite size. The chemical compositions in the MoO_3 MS_s fabricated at different temperatures are non-stoichiometric and may ordinarily consist of excess oxygen vacancies and Mo atoms. These defects can behave as nonradiative canters and reduce the emitted radiation from MoO_3 MS_s. At high growth temperature the density of such defects reduces with an improvement in crystallinity and probably supports the establishment of point defects responsible for the radiative recombinations. Rest of that, the high temperature during last growth step facilitates the migration of grain boundaries and promotes the coalescence of small crystallites consequently surface to volume ratio decreases with the increase of crystallite size, and the larger grains have smaller nonradiative relaxation rates over the surface states. As a result, the of process non radiative relaxation occurring in the surface states will remarkably increase the PL intensity [41–43].

4. Conclusion

In summary, uniformly distributed molybdenum oxide MoO_3 MS_s are synthesized on nickel coated glass substrate by the facile PVD process, which include the plasma assisted sublimation and thermal evaporation process in three independent steps. We have studied the influence of substrate temperature during last growth step on the structural, surface morphological, vibrational and optical properties of MoO_3 MS_s. SEM and TEM studies ascertain the gradual formation of fine microspheres with different substrate temperature. The XRD, Raman, and FTIR analysis are revealed that MoO_3 MS_s grown at distinct temperatures have single orthorhombic phase. The measured crystallite size of films obtained by Debye–Scherrer formula nearly matched with TEM observations particularly at high growth temperature. The significantly enhanced crystallite size with the substrate temperature, assured the improvement in degree of crystallinity. Raman and FTIR studies divulge that the vibrational properties of MS_s are depending on the substrate temperature and coincide with XRD findings. The MoO_3 MS_s show room temperature PL emission in the UV–visible region. The substrate temperature has strongly influenced the light emission characteristics of MoO_3 MS_s. The ability to produce the molybdenum oxide MS_s in thin films with reproducible structural, morphological and, optical characteristics should be useful for the application of gas sensing, photo-chromic devices and highly efficient lithium ion batteries.

Acknowledgement

One of the authors Rabindar K. Sharma gratefully acknowledges the financial assistance from Council of Scientific and Industrial Research (CSIR)-India.

References

[1] Y. Xia, P. Yang, Y. Sun, Y. Wu, B. Mayers, B. Gates, Y. Yin, F. Kim, H. Yan, Adv. Mater. 15 (2003) 353.
[2] Hua Gui Yang, Hua Chun Zeng, Angew Chem. Int. Ed. 43 (2004) 5930.
[3] Xiaowei. Teng, Hong. Yang, Nano Lett. 5 (2005) 885.
[4] Changlong Jiang, Wangqun Zhang, Yankuan Liu, Yitai Qian, Cryst. Growth Des. 6 (2006) 2603.
[5] Gutao Duan, Weiping Cai, Yuanyuan Luo, Zhigang Li, Yue Li, Appl. Phys. Lett. 89 (2006) 211905.
[6] Yingjie Feng, Mei Zhang, Min Guo, Xidong Wang, Cryst. Growth Des. 10 (2010) 1500.
[7] Hu Lin, Hao Zhong, Xinrui Zheng, Yimin Huang, Ping Zhang, Qianwang Chen, Sci. Rep. 2 (2012) 986.
[8] Jingjing Liu, Manickam Sasidharan, Dian Liu, Yuuichi Yokoyama, Shin-ichi Yusa, Kenichi Nakashima, Mater. Lett. 66 (2012) 25.
[9] Andrea Ponzoni, Elisabetta Comini, Giorgio Sberveglieri, Jun Zhou, Shao Zhi Deng, Ning Sheng Xu, Yong Ding, Zhong Lin Wang, Appl. Phys. Lett. 88 (2006) 203101.
[10] Tarsame S. Sian, G.B. Reddy, J. Appl. Phys. 98 (2005) 026104.
[11] F.F. Ferreira, Tersio G. Souza Cruz, M.C.A. Fantini, M.H. Tabacniks, Sandra C. de Castro, Jonder Morais, Abner de Siervo, Richard Landers, A. Gorenstein, Solid State Ionics 136 (2000) 357.
[12] M.A.Q. Lopez, R.F. Reidy, R.A.O. Teran, O.M. Gonzalez, R.R. Bon, J. Mater. Sci. Mater. Electron. 11 (2000) 151.
[13] A.M. Anderson, C.G. Granquvist, J.R. Stevens, Appl. Opt. 28 (1989) 3295.
[14] C.G. Granqvist, Solid State Ionics 53 (1992) 479.
[15] M. Ferroni, V. Guidi, G. Martinelli, P. Nelli, M. Sacerdoti, G. Sberveglieri, Thin Solid Films 307 (1997) 148.
[16] H. Al-Kandari, F. Al-Khorafi, H. Belatel, A. Katrib, Catal. Commun. 5 (2004) 225.
[17] M. Hashimoto, S. Watanuki, N. Koshida, M. Komuro, N. Atoda, Japan, J. Appl. Phys. 35 (1996) 3665.
[18] Jun Zhou, S.Z. Deng, N.S. Xu, Jun Chen, J.C. She, Appl. Phys. Lett. 83 (2003) 2653.
[19] D.E. Diaz-Droguett, V. M Fuenzalida, G. Solorzano, J. Nanosci. Nanotechnol. 8 (2008) 5977.
[20] E. Redel, R. Thomann, C. Janiak, Chem. Commun. (2008) 1789–1791.
[21] N.A. Dhas, K.S. Suslick, J Am. Chem. Soc. 127 (2005) 2368.
[22] Yuanyuan Li, Jinping Liu, Xintang, Guangyan Li, Cryst. Growth Des. 7 (2007) 7.
[23] D.B. Cullity, Element of X-ray Diffraction, Reading, MA, Addision-Wesley, 1956.
[24] M. Dieterle, G. Mestl, Phys. Chem. Chem. Phys. 4 (2002) 822.
[25] G. Andersson, A. Magneli, Acta Chem. Scand. 4 (1969) 793.
[26] L. Kihlborg, Ark. Kemi. 21 (1963) 357.
[27] I.R. Beattie, T.R. Gilson, J. Chem. Soc. A (1969) 2322.
[28] G. Mestl, N.F.D. Verbruggen, E. Bosch, H. Knozinger, Langmuir 12 (1996) 2961.
[29] G.M. Ramans, J.V. Gabrusenoks, A.R. Lusis, A.A. Patmalnieks, J. Non-Cryst. Solids 90 (1987) 637.
[30] M.A. Py, K. Maschke, Physica B 105 (1981) 376.
[31] K. Srinivasa Rao, B. Rajini Kanth, P.K. Mukhopadhyay, Appl. Phys. A 96 (2009) 985.
[32] T.S. Sain, G.B. Reddy, Appl. Surf. Sci. 236 (2004) 1.
[33] M. Anwar, C.A. Hogarth, C.R. Theocharis, J. Mater. Sci. 24 (1989) 2387.
[34] K. Rabindar Sharma, G.B. Reddy, AIP Adv. 3 (2013) 092112.
[35] K. Rabindar Sharma, G.B. Reddy, J. Appl. Phys. 114 (2013) 184310.
[36] J. Song, X. Ni, D. Zhang, H. Zheng, Solid State Sci. 8 (2006) 1164.
[37] M. Itoh, K. Hayakawa, S. Oishi, J. Phys. Condens. Matter 13 (2001) 5853.
[38] R. Erre, M.H. Legay, J.J. Fropiat, Surf. Sci. 127 (1983) 69.
[39] M. Dieterle, G. Weinberg, G. Mestl, Phys. Chem. Chem. Phys. 4 (2002) 812.
[40] M. Labanowaka, Phys. Chem. Chem. Phys. 1 (1999) 5385.
[41] Y.G. Yang, S.P. Lau, H.W. Lee, S.F. Yu, S.K. Tay, X.Z. Zang, H.H. Hing, J. Appl. Phys. 94 (2003) 354.
[42] T. Matsumoto, H. Kato, K. Miyamoto, M. Sano, T. Yao, Appl. Phys. Lett. 81 (2002) 1231.
[43] L.H. Quang, S.J. Chua, K.P. Loh, E. Fitzgerald, J. Cryst. Growth 287 (2006) 157.